Fast and Tissue-Optimized Mapping of Magnetic Susceptibility and T2* with Multi-Echo and Multi-Shot Spirals

Bing Wu[1], **Wei Li**[1], **Alexandru Vlad Avram**[1,3], **Sung-Min Gho**[1,4], and **Chunlei Liu**[1,2,*]

[1]Brain Imaging and Analysis Center, Duke University, Durham NC

[2]Department of Radiology, School of Medicine, Duke University, Durham NC

[3]Biomedical Engineering Department, Pratt School of Engineering, Duke University, Durham NC

[4]Department of Electrical and Electronic Engineering, Yonsei University, Seoul, Republic of Korea

Abstract

Gradient-echo MRI of resonance-frequency shift and T2* values exhibits unique tissue contrast and offers relevant physiological information. However, acquiring 3D-phase images and T2* maps [A1] with the standard spoiled gradient echo (SPGR) sequence is lengthy for routine imaging at high-spatial resolution and whole-brain coverage. In addition, with the standard SPGR sequence, optimal signal-to-noise ratio (SNR) cannot be achieved for every tissue type given their distributed resonance frequency and T2* value. To address these two issues, a SNR optimized multi-echo sequence with a stack-of-spiral acquisition is proposed and implemented for achieving fast and simultaneous acquisition of image phase and T2* maps. The analytical behavior of the phase SNR is derived as a function of resonance frequency, T2* and echo time. This relationship is utilized to achieve tissue optimized SNR by combining phase images with different echo times. Simulations and *in vivo* experiments were designed to verify the theoretical predictions. Using the multi-echo spiral acquisition, whole-brain coverage with 1 mm isotropic resolution can be achieved within 2.5 minutes, shortening the scan time by a factor of 8. The resulting multi-echo phase map shows similar SNR to that of the standard SPGR. The acquisition can be further accelerated with non-Cartesian parallel imaging. The technique can be readily extended to other multi-shot readout trajectories besides spiral. It may provide a practical acquisition strategy for high resolution and simultaneous 3D mapping of magnetic susceptibility and T2*.

Keywords

Image phase; susceptibility map; fast imaging; spiral; multiple echoes

INTRODUCTION

Recent advances in scanner hardware and signal processing techniques have allowed the diagnostic value of the image phase (or resonance frequency shift) to be better exploited. For example, Rauscher et al demonstrated that image phase reveals contrast in the deep nucleus

*Correspondence Address: Chunlei Liu, Ph.D., Brain Imaging and Analysis Center, Duke University School of Medicine, 2424 Erwin Road, Suite 501, Campus Box 2737, Durham, NC 27705, Phone: (919)681 4788, Fax: (919)681 7033, chunlei.liu@duke.edu.

regions that is not observed in the corresponding magnitude images (Rauscher et al., 2005); Duyn et al reported that the phase images provide better contrast at the white matter and gray matter interface than the magnitude images (Duyn et al., 2007; Lee et al., 2010). Image phase also allows susceptibility maps to be derived. Compared to image phase, susceptibility is an intrinsic local tissue property that can be measured quantitatively. Quantitative susceptibility measurement potentially allows assessment of iron and myelin tissue contents (Li et al., 2011). Iron content in the deep nucleus is an indicator for various neurodegenerative diseases (Haacke et al., 2005) such as Parkinson's disease (PD), Alzheimer's disease (AD) and Huntington's disease.

Quantitative susceptibility mapping requires 3D volume coverage. Commonly, the image phase information is obtained with a 3D spoiled-gradient echo sequence (SPGR). However, due to the desired long echo time (TE) and high isotropic resolution, whole brain imaging is often a prolonged process. For instance, it takes approximately 20 minutes to acquire images with 1 mm isotropic resolution ($192 \times 192 \times 120$ volume) and a TR of 52ms. Such long scan time gives rise to many motion related artifacts. This long scan time becomes impractical for multi-orientation based susceptibility mapping (Liu et al., 2009; Wharton and Bowtell, 2010) and for susceptibility tensor imaging (Liu, 2010). Although under-sampling techniques such as parallel imaging (Pruessmann et al., 1999; Wu et al., 2009) and compressed sensing (Lustig et al., 2007; Wu et al., 2011) may be potentially incorporated to reduce scan time, the reconstructed image is always afflicted with artifacts such as noise amplification and loss of image contrast and details. Furthermore, brain tissues typically have a wide range of frequency shifts and T2* values, resulting in different signal behavior for different tissue types. For example, deep nuclei exhibit positive frequency shift and short T2* while white matter shows negative frequency shift and relatively long T2*. Consequently, optimal measurement of frequency shift and magnetic susceptibility cannot be achieved with the standard SPGR method. In summary, faster and tissue-optimized imaging techniques are necessary to resolve these important issues.

Here, we propose a multi-echo multi-shot technique to achieve faster image acquisition and tissue-optimized signal-to-noise ratio (SNR). Although a spiral trajectory is utilized in the current implementation, other multi-shot trajectories, such as multi-shot EPI and read-out segmented EPI, can be readily incorporated. Due to its efficient use of the field gradient system, the spiral readout trajectory allows the k-space to be traversed rapidly and efficiently. In addition to fast imaging benefit, spiral imaging also has other intrinsic properties compared to Cartesian trajectories, such as SNR efficiency and inherent refocusing of motion- and flow-induced phase error (Delattre et al., 2010). Due to these properties, spiral imaging has been widely employed in Cardiac imaging (Ryf et al., 2004), diffusion tensor imaging (Liu et al., 2004), coronary artery imaging (Kressler et al., 2007) and functional MRI (Hu and Glover, 2007; Truong and Song, 2008) when high temporal resolution is required and motion is a potential problem. The drawback of spiral sampling compared to Cartesian sampling, however, is the increased susceptibility to off-resonance artifacts. When a short readout time is used, the off-resonance distortion can be limited and image phase information can be captured equally well as in Cartesian sampling. To improve and optimize SNR, we derive an optimal strategy to combine multi-echo data following the signal behavior that is specific to the underlying tissue properties (frequency shift and T2*). Multi-echo acquisition during the otherwise unused time interval does not require extra scan time. Multi-echo fMRI has been shown to increase the sensitivity of BOLD signal detection (Posse et al., 1999) whereas the use of multiple echo data set in the SWI shows improved SNR and contrast-to-noise (CNR) in the vascular regions (Denk and Rauscher, 2010).

The aim of this work is to achieve fast and accurate phase, susceptibility and T2* imaging based on a multi-echo spiral sequence. The temporal characteristics of the phase SNR at

different echo times is investigated and used to optimally combine phase images and achieve tissue-optimized SNR. Phase imaging at a very high resolution (0.5 mm isotropic) using the proposed method is demonstrated at 3.0 T.

THEORY

SNR of Image phase at a Single Echo

The Rician noise in the magnitude of MR signal is typically approximated as additive white noise in the limit of high SNR. In gradient echo, the SNR of signal magnitude decays exponentially as characterized by the T2* tissue relaxation time, and hence the shortest echo time is most desirable for maximal SNR of the magnitude. However, the SNR behavior of the image phase is less intuitive as it is non-linear and is a function of both resonance frequency and T2*. In other words, the phase behavior is tissue dependent. An exact knowledge of this behavior can be useful for optimizing the echo time to maximize phase SNR.

The MR signal M at time t may be written as:

$$M = M_0 e^{-\frac{t}{T2^*}} e^{-j2\pi ft} + n = M_0 e^{-\frac{t}{T2^*}} \cos(2\pi ft) - jM_0 e^{-\frac{t}{T2^*}} \sin(2\pi ft) + n_{re} - jn_{im} \quad (2)$$

Where n_{re} and n_{im} represents white noise in real and imaginary parts with the same noise power, M_0 is the transverse magnetization, j is the imaginary unit and f is the frequency offset. It can be shown that the noise in signal phase, n_θ, in a first-order approximation, may be written as (see Appendix):

$$n_\theta = \frac{1}{M_0 e^{-\frac{t}{T2^*}}} n_{im} \cos(2\pi ft) - j\frac{1}{M_0 e^{-\frac{t}{T2^*}}} n_{re} \sin(2\pi ft) \quad (7)$$

If the real and imaginary channel has equal noise variance, i.e. if $\sigma_{re}^2 = \sigma_{im}^2 = \sigma^2$, the noise power in the phase is:

$$\sigma_\theta^2 = \left(\frac{1}{M_0 e^{-\frac{t}{T2^*}}} \sigma\right)^2 \quad (8)$$

Then the SNR of the image phase at time t may be written as:

$$SNR_\theta = \frac{2\pi ft}{\sigma_\theta} = \frac{2\pi ftM_0 e^{-\frac{t}{T_2^*}}}{\sigma} \quad (9)$$

It shows that the SNR of the image phase is dependent on the frequency offset source, the transverse magnetization, and the T2* tissue relaxation time. It is then easy to derive the echo time at which the phase SNR is optimal:

$$\frac{dSNR_\theta}{dt} = 0 \implies t = t_2^* \quad (10)$$

The image phase reaches its maximal SNR when the echo time is equal to T2*.

Tissue-Optimized SNR of Resonance Frequency with Multiple Echoes

Resonance frequency shift at different TEs [A2] can be calculated by normalizing the phases with their respective TE. Notice that, at a given TE, the SNR of frequency is the same as the SNR of phase as they are related by a constant scaling factor. Assuming that the noise levels in the phase images acquired with different echo times are temporally uncorrelated, a straight forward algebraic averaging improves the SNR level. Based on Eq. (9), direct averaging of the frequencies at N echoes leads to a SNR of:

$$SNR_{ME} = \frac{2\pi f}{\sqrt{\sum_{n=1}^{N} \frac{1}{(M_{t_n} t_n)^2}} \sigma}$$

(11)

Where t_n denotes the n-th TE out of the N echoes, and $M_{t_n} = M_0 e^{-\frac{t}{T_2^*}}$ denotes the signal magnitude at t_n. An optimal way of combining the frequencies measured at different TE is to weigh the frequencies with their respective SNR prior to the combination, similar to that used in fMRI (Posse et al., 1999). Specifically, the frequency map at echo time t_n is weighted by:

$$W_n = \frac{t_n e^{-\frac{t_n}{T_2^*}}}{\sum_{n=1}^{N} t_n e^{-\frac{t_n}{T_2^*}}}$$

(12)

In this way, the SNR of the weighted combination is given as:

$$SNR_{MEW} = \frac{\sum_{n=1}^{N} M_{t_n} t_n \bullet 2\pi f}{\sqrt{n}\delta}$$

(13)

We refer the above two ways of calculating resonance frequency as multi-echo (ME) averaging and multi-echo weighted (MEW) averaging respectively.

Calculating the SNR of multi-echo weighted frequency using Eq.(13) requires knowledge of M_0, f and T2*. It is more informative to calculate the SNR ratios when comparing the two SNRs. The ratios of the SNR gains from multi-echo acquisition by using (11) and (13) are:

$$\frac{SNR_{ME}}{SNR_{t_2^*}} = \frac{N}{0.37 t_2^* \sqrt{\sum_{n=1}^{N} \frac{1}{(t_n e^{-\frac{t_n}{t_2^*}})^2}}}$$

(14)

$$\frac{SNR_{MEW}}{SNR_{t_2^*}} = \frac{\sum_{n=1}^{N} t_n e^{-\frac{t_n}{t_2^*}}}{0.37 \sqrt{N} t_2^*}$$

(15)

In Eq. (14) and (15), only the T2* of the tissues are needed for calculating SNR gains. For a T2* of 30 ms, the theoretical SNR gains by combining the frequency maps at 10 ms, 20 ms, 30 ms, 40 ms and 50 ms are 1.88 and 1.96 respectively for multi-echo averaging and multi-echo weighted averaging. These gains are approximately equivalent to the SNR gain that can be obtained from averaging 4 acquisitions (a gain of 2).

METHODS

Simulation

Simulations were conducted to investigate the characteristics of phase SNR and the SNR levels of phase images acquired with a multi-echo sequence in comparison to those of single-echo phases. A complex MR signal with a given frequency offset and T2* relaxation time was simulated with white noise added to the real and imaginary parts respectively. The temporal variation of the MR signal within 0 ms and 60 ms was then simulated and the signal phase was extracted. To calculate the phase SNR, 50000 independent samples of the signal were generated and the phase SNR at a given time point was calculated as the ratio of the mean phase value to the standard deviation.

The SNR calculations were repeated for a range of frequency offsets (2 Hz to 10 Hz in steps of 2 Hz) and T2* relaxation times (10 ms to 50 ms in steps of 10 ms). [A3] The SNR of the resonance frequency obtained by averaging the resonance frequency simulated with different echo times was compared to that of the resonance frequency simulated with TE=T2*, i.e. where the phase SNR is expected to be maximum. Both multi-echo averaging and multi-echo weighted averaging were considered.

In Vivo Experiments

The sequence shown in Figure 1a was implemented, i.e. five equidistant spiral-out trajectories were concatenated with a separation of 10 ms with a minimum echo time of 8ms[A4]. A uniform density spiral trajectory consisting of 18 interleaves was used with a 8.4 ms readout duration (Glover, 1999). *In vivo* brain imaging of three healthy adult volunteers [A5]was performed on a 3T GE MR750 scanner (GE Healthcare, Waukesha, MI) equipped with an 8 channel head coil. Written informed consent was obtained from each subject in compliance with a protocol approved by the Institutional Review Board. Complex images were reconstructed with standard gridding and sampling density compensation calculated using the Voronoi method (Rasche et al., 1999) for each coil and independently processed as follows. Phase data were first extracted and unwrapped using an algorithm based on the Laplace operator (Li et al., 2011). Next, background phase removal was performed using the sphere mean value (SMV) filter (Schweser et al., 2011). The resulting phase maps from each coil were then averaged to obtain the final phase map.

In vivo assessment of SNR—To assess the SNR behavior of the phase, two scans were performed each with the first echo starting at 10 ms and 15 ms respectively. In this way, phase images were obtained at a set of echo times ranging from 10 ms to 55 ms with a 5 ms separation. For both scans the following scan parameters were used: TR = 70 ms, flip angle = 20°, FOV = $192 \times 192 \times 30$ mm^3 and matrix size = $192 \times 192 \times 30$ which resulted in an isotropic 1 mm resolution. Each scan was repeated 20 times and the phase SNR was calculated as the ratio of the mean phase to the standard deviation of the phase across the 20 repetitions. Then resonance frequency shift maps were calculated using either phase maps acquired with different echo times or by combining the frequency shifts estimated at different echo times using weighed averaging. The SNRs of the resulting frequency shift maps were calculated for selected region-of-interest in white matter, grey matter and CSF. Due to the inhomogeneity of the frequency shifts within different tissues, the ROIs were

manually selected based on the frequency shift map and constrained to several voxels. In the multi-echo weighted averaging, the T2* relaxation time needed for calculating the weights was determined by fitting the signal to an exponential decay curve.

Comparison with SPGR—A second experiment was carried out to compare the frequency shift and susceptibility maps obtained using the multi-echo spiral acquisitions to that obtained using the standard 3D SPGR sequence. The following scan parameters were used in the spiral acquisition: TR = 70 ms, flip angle = 20°, FOV = $192 \times 192 \times 120$ mm^3 and matrix size = $192 \times 192 \times 120$ which resulted in an isotropic 1 mm resolution. The first echo acquisition was at 10 ms. A scan using GE's product 3D SPGR sequence was performed on the same subject, using identical parameters as in the multi-echo spiral sequence with TE/TR = 40/52 ms. The scan time for SPGR was 20 minutes whereas that of the multi-echo spiral sequence was only 2.5 minutes. After phase processing, susceptibility maps were calculated from the different phase maps using the LSQR method as described previously (Li et al., 2011). The quantitative susceptibility values of different tissue regions were computed by using the susceptibility of CSF as a reference, i.e. the difference between the susceptibility values of a given region of interest (ROI) and that of the CSF region. Segmentation of the deep nuclei regions was performed manually using susceptibility maps and magnitude images as reference. [A6]

R2* mapping—Using the 3D data set ($192 \times 192 \times 120$) described in the previous section, R2* maps were computed by fitting a mono-exponential decay curve [A7]to the magnitude images acquired with different echo times[A8]. [A9]The relationship between the R2* and susceptibility values was investigated in selected deep nucleus regions with a standard correlation analysis.

Parallel imaging—Parallel imaging was applied to further accelerate the scan: the full spiral data set acquired in the second experiment [A10]was under-sampled with an acceleration factor of 2 by discarding every other interleave [A11]. The central 40 k_z planes [A12] were fully sampled and used to obtain the coil sensitivity profiles. Image reconstruction for data acquired at each echo time was performed with the projection-on-convex SENSE (POC SENSE) (Samsonov et al., 2004) method based on the conjugate gradient algorithm. The stopping criterion was set to be a residual error of 0.001. The resulting frequency map was calculated with multi-echo weighed averaging and compared to that of the fully sampled data set.

High resolution phase imaging—The fast data acquisition and inherently high SNR of the multi-echo spiral technique allows practical high-resolution phase imaging. To evaluate its performance at high spatial resolution, additional images were acquired with the following parameters: FOV = 192 mm, matrix size = 384×384, 64 interleaves resulting in a 0.5 mm resolution. As a comparison, lower resolution images were acquired on the same subject with a matrix size of 192×192 and a resolution of 1.0 mm. In both cases, the length of spiral readout trajectory is maintained as close as possible with 8.5 ms for 0.5 mm resolution and 8.4 ms for 1.0 mm resolution, allowing equal echo spacing[A13], same TEs and TR for both cases. As a result, both acquisitions have the same SNR gains from multi-echo weighted averaging and equivalent off-resonance levels.

RESULTS

Simulation

Figure 2 shows the SNR behavior of the phase as a function of T2* and frequency shift. In Figure 2a and 2b the temporal SNR curves with varying frequency offset levels and T2*

times are shown respectively. In Figure 2a the frequency offset was varied from 2 Hz to 10 Hz with a 2 Hz increment while the T2* was fixed at 30 ms; in Figure 2b, the T2* was varied from 20 ms to 50 ms in 10 ms[A14] increments while the frequency offset was fixed at 6 Hz. From Figure 2a, it is seen that the phase SNR at a given time point is linearly proportional to the frequency offset, but the frequency offset has no effect on the time at which the maximal SNR occurs. In Figure 2b, it is seen that the maximal SNR does occur at TE=T2* and is linearly proportional to the T2* relaxation time. Both observations agree well with the theoretical model in Eq.(9).

Figure 2c compares the SNR performance of multi-echo averaging and multi-echo weighted averaging in reference to single-echo acquisition. A five-echo acquisition with TE of 10 ms, 20 ms, 30 ms, 40 ms and 50 ms is shown for a frequency offset of 6 Hz and a T2* of 30 ms. The resulting resonance frequency SNR calculated from the multi-echo data are labeled in Figure 2c in comparison to the SNR of individual acquisitions at each TE. The SNR of multi-echo averaging and multi-echo weighed averaging is, respectively, 1.79 and 1.87 times of the maximal SNR obtainable with single-echo acquisition. These values are comparable to the theoretically predicted figures of 1.88 and 1.96 respectively; the slight difference between simulation and theoretical prediction is likely due to the approximation used in the model and also the insufficient number of samples.[A15]

Experiment

The analysis presented below is based on the data acquired from the same healthy volunteer. Consistent findings were observed across all three volunteers. [A16]

In vivo assessment of SNR—Figure 3a shows a set of representative frequency maps obtained at the five echo times (from 10 ms to 50 ms) and the[A17] corresponding frequency map obtained with multi-echo weighted averaging. It is seen that the image phase has a temporally and spatially varying level of contrast-to-noise-ratio (CNR). For instance, the white/grey matter contrast is more noticeable at later echo times such as in the cortex region as indicated by the arrow. On the other hand, the deep nuclei appear to have better CNR at shorter TE (comparing the red nucleus region in frequency maps obtained at 20 ms and 40 ms) due to their shorter T2* values. The multi-echo weighted averaging results in a frequency map CNR superior to that obtained with any individual echo time. Figure 3b-d shows the measured (stars) and predicted (solid lines) temporal variations of phase SNR in ROIs of white matter, grey matter and CSF respectively. The theoretically predicted SNR curves were calculated using the measured T2* relaxation times, which were 38 ms, 45 ms and 80 ms for white matter, grey matter and CSF respectively. It is evident that the measured SNR levels agree well with the theoretical predictions. Both experimental data and theoretical predications confirm that the maximal SNR occurs with TE around T2*. [A18] [A19]

Table 1 lists the predicted and measured SNR gains by using the multi-echo weighted averaging of the selected ROIs in white matter, grey matter and CSF. [A20] In the cases of white matter and grey matter, the frequency SNR values measured with echo times of 40 ms and 45 ms were used respectively (closest to the estimated T2* times); in the case of CSF, the frequency SNR of the acquisition with echo time of 55 ms was used. The multi-echo frequency shift map was obtained by combining the frequency shift maps measured at all 10 echo times[A21], using the SNR weights as in Eq.(13). The measured SNR gains are seen to be similar to the predicted gains; the difference might be due to the errors involved in estimating the SNR levels at individual echo times.

Comparison with SPGR—The frequency maps obtained from the multi-echo spiral and the SPGR sequences are compared in Figure 4a. It is seen that both frequency maps show good contrast in various brain structures such as the deep nuclei and the grey/white matter interfaces. No significant SNR differences were observed in the two maps despite the 8 fold reduction in scan time in the multi-echo spiral technique. Overall, the frequency maps obtained with the multi-echo spiral method appear to be slightly smoother than those of SPGR due to off-resonance, gridding and the circular coverage of k-space in spiral trajectory. Similar characteristics can be also observed in the calculated susceptibility maps as shown in Figure 4b. Nevertheless, the susceptibilities calculated with both sequences are very similar in iron-rich regions of deep nuclei [A22]such as the putamen (PU), the red nucleus (RN), the substantia nigra (SN) and the globus pallidus (GP)[A23] (Table 2).

R2* mapping—Figure 5.a and 5.b shows examples of multi-echo magnitude images and calculated R2* maps respectively. It is seen that high-quality magnitude images were obtained using the spiral acquisition. [A24]The R2* map shows good delineation of the deep nucleus regions, such as the RN and SN as labeled. However, the contrast between gray and white matter is not nearly as good as in resonance frequency images. Figure 5b plots the measured R2* values of four regions of deep nucleus (GP, PU, RN and SN) against their measured susceptibility values. A strong correlation is observed (correlation coefficient = 0.99).

Parallel imaging—Figure 6 compares the frequency maps extracted from the fully sampled and the parallel imaging accelerated (acceleration factor of 2) datasets. Figure 6a shows two typical fully sampled frequency maps while Figure 6b shows the corresponding frequency maps obtained with an acceleration factor of 2. In Figure 6c a line profile for each image is plotted. It can be seen that the tissue features and contrast are well maintained in frequency maps reconstructed from the under-sampled dataset, despite a slightly higher noise level, as expected.

High-resolution imaging of frequency shift—Figure 7 compares frequency maps acquired at 1 mm resolution and 0.5 mm resolution. At 0.5 mm resolution, the frequency map features finer tissue details and sharper delineation of tissue boundaries. The enhanced structural details are especially evident in regions of the white/grey matter interface and white matter fiber bundle, such as indicated in the zoom-in regions. It is evident that the proposed technique is capable of generate high-resolution maps of frequency shift at 3 T. [A25]

DISCUSSION & CONCLUSION

We have proposed and implemented a fast data acquisition strategy for simultaneous mapping of frequency shifts and T2* values at high-spatial resolution. This technique samples the T2* decay curve at multiple echoes within one TR. The measured T2* values are used to optimally combine the multi-echo data for the calculation of frequency maps. Although the current implementation utilizes a stack-of-spiral trajectory, the technique can be readily extended to other multi-shot trajectories. With the proposed method, whole-brain coverage with 1 mm isotropic resolution can be achieved at 8-times faster than the standard 3D SPGR sequence without apparent loss of image quality. Further combination with parallel imaging makes it feasible to acquire whole-brain susceptibility and T2* maps simultaneously at minute-temporal resolution.

One important issue in the frequency shift imaging is choosing the appropriate TE for a gradient echo sequence to achieve good contrast and SNR. This issue is addressed here with multi-echo acquisition and optimal data combination. We first analyzed the SNR behavior of

the phase and elucidated its dependence on resonance frequency and T2*. It is shown that the maximal phase SNR is achieved at TE = T2* which is consistent with findings in BOLD fMRI. While BOLD contrast is primarily focused on the cortical gray matter, phase contrast examines the frequency distribution in the whole brain. Cortical gray matter has relatively uniform T2* values (~ 40 ms at 3.0 T); however, brain tissues by and large have a wide range of T2* values (see Figure 5). As a result, optimal SNR cannot be achieved simultaneously for all tissue types. This problem is overcome with the proposed technique of multi-echo weighted averaging. It is shown that the resulting maps of frequency shift and corresponding magnetic susceptibility have comparable SNR and CNR to those acquired with a standard 3D SPGR sequence.

Long scan time has been a critical obstacle for routine application of quantitative susceptibility and T2* mapping. The proposed technique of multi-echo weighted averaging improves the scan efficiency by a factor of 8 without sacrificing the quantitative accuracy and image quality. It allows simultaneous mapping of magnetic susceptibility and T2* within 2.5 minutes. Further acceleration can be achieved by reducing the number of spiral interleaves and using parallel imaging. Reducing the number of interleaves, however, increases the readout length resulting in more pronounced off-resonance blurring. Off-resonance artifacts may be mitigated by performing better shimming, applying off-resonance correction or employing a susceptibility compensating RF excitation such as that in (Yang et al., 2010; Yang et al., 2011). Based on initial experiences, applying a scanner product shimming procedure and using 18 or more interleaves results in good image quality for a spatial resolution of 1 mm at 3T[A26]. Off resonance corrections using estimated field map have also been attempted on the current data set, but no obvious improvement was noticed due to the short readout time used. As demonstrated, higher resolution (0.5 mm) can be achieved with negligible artifacts and within practical scan time. The optimal combination of number of interleaves, acceleration factor and number of echoes to be used for achieving the optimal SNR and off-resonance requires further investigation.

The capability of determining susceptibility and T2* (R2*) simultaneously within one scan offers a unique opportunity to study the relationship between these two and their physiological relevance. Susceptibility and R2* may provide complementary information for tissue characterization. Both R2* (Ghugre et al., 2006; Langkammer et al., 2010; St Pierre et al., 2005) and susceptibility (Li et al., 2011; Schweser et al., 2011) have been suggested as a measure for tissue iron levels. In our in vivo data, a strong correlation was observed between R2* and susceptibility in the deep nuclei. While R2* measures the absolute rate of signal decay, susceptibility measurements are relative. Furthermore, magnetic susceptibility may not be the sole source of the observed frequency offset (Shmueli et al., 2011; Zhong et al., 2008). It is unclear how T2* is affected by the different sources that influence the phase contrast. In brain white matter, both T2* and magnetic susceptibility have been reported to depend on the underlying neuronal fiber orientation with respect to external magnetic field. The exact mechanisms are still under investigation. Studying T2* and susceptibility together may allow us to gain further insight of the brain tissue intrinsic properties.

APPENDIX

For a given signal

$$M = M_0 e^{-\frac{t}{T2^*}} \cos(2\pi f t) - j M_0 e^{-\frac{t}{T2^*}} \sin(2\pi f t) + n_{re} - j n_{im} \qquad [A1]$$

Denote the signal magnitude $M_t = M_0 e^{-\frac{t}{T2^*}}$, then the real and imaginary parts are:

$$M_{re} = M_t \cos(2\pi ft) + n_{re}$$
$$M_{im} = M_t \cos(2\pi ft) + n_{im}$$

Denote the signal phase $\theta = 2\pi ft$ and the noise impaired signal phase $\hat{\theta} = 2\pi ft + n_\theta$, then

$$\cos(\widehat{\theta}) = \frac{M_{re}}{|M_{re} + iM_{im}|} = \frac{M_t \cos(\theta) + n_{re}}{\sqrt{(M_t \cos(\theta) + n_{re})^2 + (M_t \sin(\theta) + n_{im})^2}}$$
$$= \frac{\cos(\theta) + \frac{1}{M_t} n_{re}}{\sqrt{1 + 2\frac{1}{M_t} n_{re} \cos(\theta) + 2\frac{1}{M_t} n_{im} \sin(\theta)}}$$
$$\approx -\frac{1}{2}\cos(\theta)(2\frac{1}{M_t}\cos(\theta)n_{re} + 2\frac{1}{M_t}\sin(\theta)n_{im}) + \frac{1}{M_t}n_{re} + \cos(\theta)$$
$$= \frac{1}{M_t}\sin^2(\theta)n_{re} - \frac{1}{M_t}\sin(\theta)\cos(\theta)n_{im} + \cos(\theta) \qquad [A2]$$

Also

$$\cos(\widehat{\theta}) = \cos(\theta + n_\theta) \approx \cos(\theta) - n_\theta \sin(\theta) \qquad [A3]$$

Combining [A3] and [A2] gives

$$n_\theta \sin(\theta) = \frac{1}{M_t}\sin^2(\theta)n_{re} - \frac{1}{M_t}\sin(\theta)\cos(\theta)n_{im}$$
$$n_\theta = \frac{1}{M_t}\sin(\theta)n_{re} - \frac{1}{M_t}\cos(\theta)n_{im} \qquad [A4]$$

Acknowledgments

References

Delattre BMA, Heidemann RM, Crowe LA, Vallee JP, Hyacinthe JN. Spiral demystified. Magnetic Resonance Imaging. 2010; 28:862–881. [PubMed: 20409660]

Denk C, Rauscher A. Susceptibility weighted imaging with multiple echoes. Journal of Magnetic Resonance Imaging. 2010; 31:185–191. [PubMed: 20027586]

Duyn JH, van Gelderen P, Li TQ, de Zwart JA, Koretsky AP, Fukunaga M. High-field MRI of brain cortical substructure based on signal phase. Proc Natl Acad Sci U S A. 2007; 104:11796–11801. [PubMed: 17586684]

Ghugre NR, Enriquez CM, Gonzalez I, Nelson MD, Coates TD, Wood JC. MRI detects myocardial iron in the human heart. Magnetic Resonance in Medicine. 2006; 56:681–686. [PubMed: 16888797]

Glover GH. Simple analytic spiral K-space algorithm. Magnetic Resonance in Medicine. 1999; 42:412–415. [PubMed: 10440968]

Haacke EM, Chengb NYC, House MJ, Liu Q, Neelavalli J, Ogg RJ, Khan A, Ayaz M, Kirsch W, Obenaus A. Imaging iron stores in the brain using magnetic resonance imaging. Magnetic Resonance Imaging. 2005; 23:1–25. [PubMed: 15733784]

Hu Y, Glover GH. Three-dimensional spiral technique for high-resolution functional MRI. Magnetic Resonance in Medicine. 2007; 58:947–951. [PubMed: 17969117]

Kressler B, Spincemaille P, Nguyen TD, Cheng L, Hai ZX, Prince MR, Wang Y. Three-dimensional Cine Imaging using variable-density spiral trajectories and SSFP with application to coronary artery angiography. Magnetic Resonance in Medicine. 2007; 58:535–543. [PubMed: 17763360]

Langkammer C, Krebs N, Goessler W, Scheurer E, Ebner F, Yen K, Fazekas F, Ropele S. Quantitative MR imaging of brain iron: a postmortem validation study. Radiology. 2010; 257:455–462. [PubMed: 20843991]

Lee J, Hirano Y, Fukunaga M, Silva AC, Duyn JH. On the contribution of deoxy-hemoglobin to MRI gray-white matter phase contrast at high field. Neuroimage. 2010; 49:193–198. [PubMed: 19619663]

Li W, Wu B, Liu C. Quantitative susceptibility mapping of human brain reflects spatial variation in tissue composition. Neuroimage. 2011; 55:1645–1656. [PubMed: 21224002]

Liu C. Susceptibility Tensor Imaging. Magnetic Resonance in Medicine. 2010; 63:1471–1477. [PubMed: 20512849]

Liu C, Bammer R, Kim DH, Moseley ME. Self-navigated interleaved spiral (SNAILS): Application to high-resolution diffusion tensor imaging. Magnetic Resonance in Medicine. 2004; 52:1388–1396. [PubMed: 15562493]

Liu T, Spincemaille P, de Rochefort L, Kressler B, Wang Y. Calculation of Susceptibility Through Multiple Orientation Sampling (COSMOS): A Method for Conditioning the Inverse Problem From Measured Magnetic Field Map to Susceptibility Source Image in MRI. Magnetic Resonance in Medicine. 2009; 61:196–204. [PubMed: 19097205]

Lustig M, Donoho D, Pauly JM. Sparse MRI: The application of compressed sensing for rapid MR imaging. Magnetic Resonance in Medicine. 2007; 58:1182–1195. [PubMed: 17969013]

Posse S, Wiese S, Gembris D, Mathiak K, Kessler C, Grosse-Ruyken ML, Elghahwagi B, Richards T, Dager SR, Kiselev VG. Enhancement of BOLD-contrast sensitivity by single-shot multi-echo functional MR imaging. Magnetic Resonance in Medicine. 1999; 42:87–97. [PubMed: 10398954]

Pruessmann KP, Weiger M, Scheidegger MB, Boesiger P. SENSE: Sensitivity encoding for fast MRI. Magnetic Resonance in Medicine. 1999; 42:952–962. [PubMed: 10542355]

Rasche V, Proksa R, Sinkus R, Bornert P, Eggers H. Resampling of data between arbitrary grids using convolution interpolation. Ieee Transactions on Medical Imaging. 1999; 18:385–392. [PubMed: 10416800]

Rauscher A, Sedlacik J, Barth M, Mentzel HJ, Reichenbach JR. Magnetic susceptibility-weighted MR phase imaging of the human brain. AJNR Am J Neuroradiol. 2005; 26:736–742. [PubMed: 15814914]

Ryf S, Kissinger KV, Spiegel MA, Bornert P, Manning WJ, Boesiger P, Stuber M. Spiral MR myocardial tagging. Magnetic Resonance in Medicine. 2004; 51:237–242. [PubMed: 14755646]

Samsonov AA, Kholmovski EG, Parker DL, Johnson CR. POCSENSE: POCS-based reconstruction for sensitivity encoded magnetic resonance imaging. Magnetic Resonance in Medicine. 2004; 52:1397–1406. [PubMed: 15562485]

Schweser F, Deistung A, Lehr BW, Reichenbach JR. Quantitative imaging of intrinsic magnetic tissue properties using MRI signal phase: An approach to in vivo brain iron metabolism? Neuroimage. 2011; 54:2789–2807. [PubMed: 21040794]

Shmueli K, Dodd SJ, Li TQ, Duyn JH. The contribution of chemical exchange to MRI frequency shifts in brain tissue. Magnetic Resonance in Medicine. 2011; 65:35–43. [PubMed: 20928888]

St Pierre TG, Clark PR, Chua-Anusorn W, Fleming AJ, Jeffrey GP, Olynyk JK, Pootrakul P, Robins E, Lindeman R. Noninvasive measurement and imaging of liver iron concentrations using proton magnetic resonance. Blood. 2005; 105:855–861. [PubMed: 15256427]

Truong TK, Song AW. Single-shot dual-z-shimmed sensitivity-encoded Spiral-in/out imaging for functional MRI with reduced susceptibility artifacts. Magnetic Resonance in Medicine. 2008; 59:221–227. [PubMed: 18050341]

Wharton S, Bowtell R. Whole-brain susceptibility mapping at high field: A comparison of multiple- and single-orientation methods. Neuroimage. 2010; 53:515–525. [PubMed: 20615474]

Wu B, Millane RP, Watts R, Bones PJ. Improved matrix inversion in image plane parallel MRI. Magnetic Resonance Imaging. 2009; 27:942–953. [PubMed: 19269768]

Wu B, Millane RP, Watts R, Bones PJ. Prior estimate-based compressed sensing in parallel MRI. Magnetic Resonance in Medicine. 2011; 65:83–95. [PubMed: 21031492]

Yang C, Deng W, Alagappan V, Wald LL, Stenger VA. Four-dimensional spectral-spatial RF pulses for simultaneous correction of B1+ inhomogeneity and susceptibility artifacts in T2*-weighted MRI. Magnetic Resonance in Medicine. 2010; 64:1–8. [PubMed: 20577982]

Yang C, Deng W, Stenger VA. Simple analytical dual-band spectral-spatial RF pulses for B(1) + and susceptibility artifact reduction in gradient echo MRI. Magnetic Resonance in Medicine. 2011; 65:370–376. [PubMed: 21264930]

Zhong K, Leupold J, von Elverfeldt D, Speck O. The molecular basis for gray and white matter contrast in phase imaging. Neuroimage. 2008; 40:1561–1566. [PubMed: 18353683]
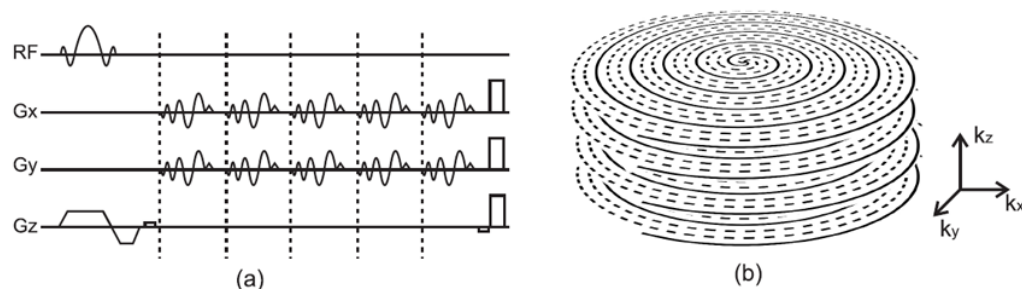
Figure 1.
Pulse sequence diagram. (a) Waveforms of the multi-echo spiral sequence. Following a 3D excitation and a z-encoding blip, a series of identical spiral-out readouts are placed at equidistant echo times. Each spiral is fully balanced and a gradient spoiler is placed at the end of the last readout. (b) A uniform density stack of spiral consisted of 18 interleaves in plane, and for display clarity only 3 interleaves are illustrated. Within a single TR, the same spiral interleave at the same z-plane is played out at incrementing TEs. Multiple TRs cycle through different interleaves and then different z-plane locations. In the end, multiple stack-of-spiral data sets are obtained at incrementing TEs. [A27]
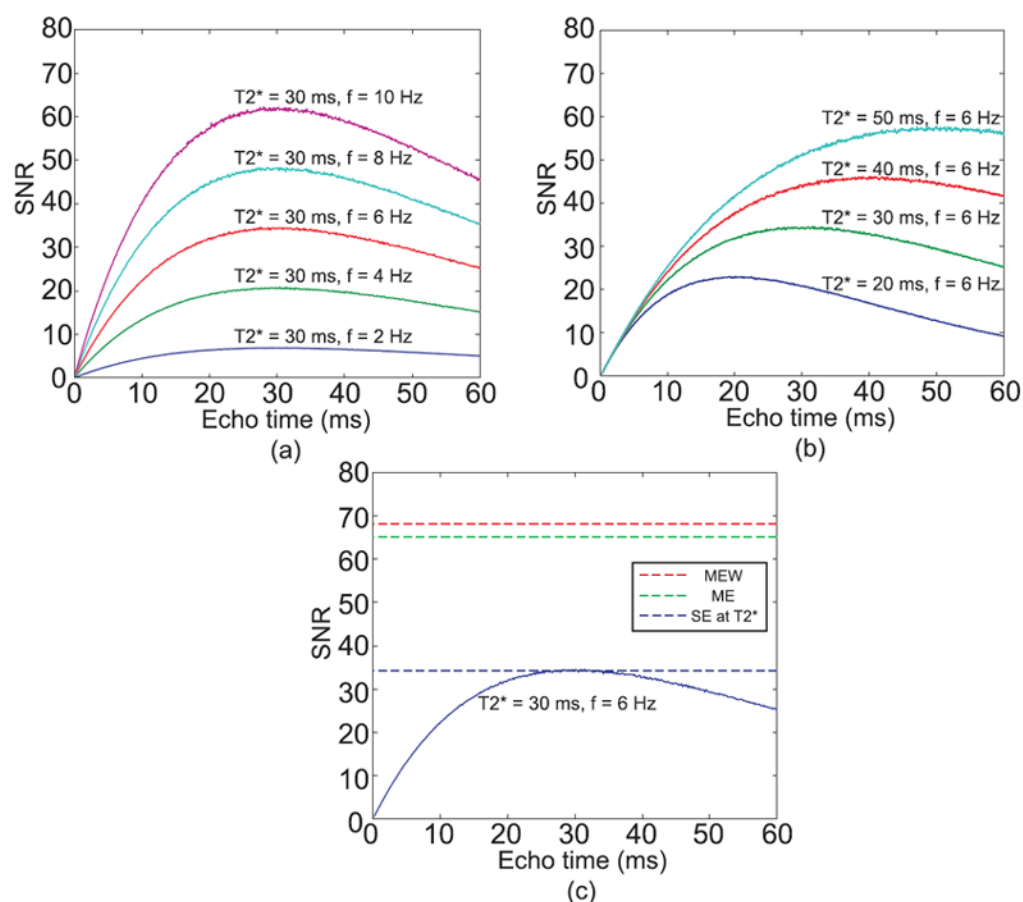
Figure 2.
Simulation results showing the behavior of phase SNR. (a) Phase SNR as a function of the echo time at different frequency offsets (2 Hz to 10 Hz in a step of 2 Hz). (b) Phase SNR as a function of the echo time for different T2* times (20 ms to 50 ms in a step of 10 ms). (c) Comparison of phase SNR of multi-echo (ME) averaging, multi-echo weighted (MEW) averaging (echo times: 10, 20, 30, 40 and 50 ms) and a single echo at the T2* (30 ms). MEW achieves the maximal SNR.
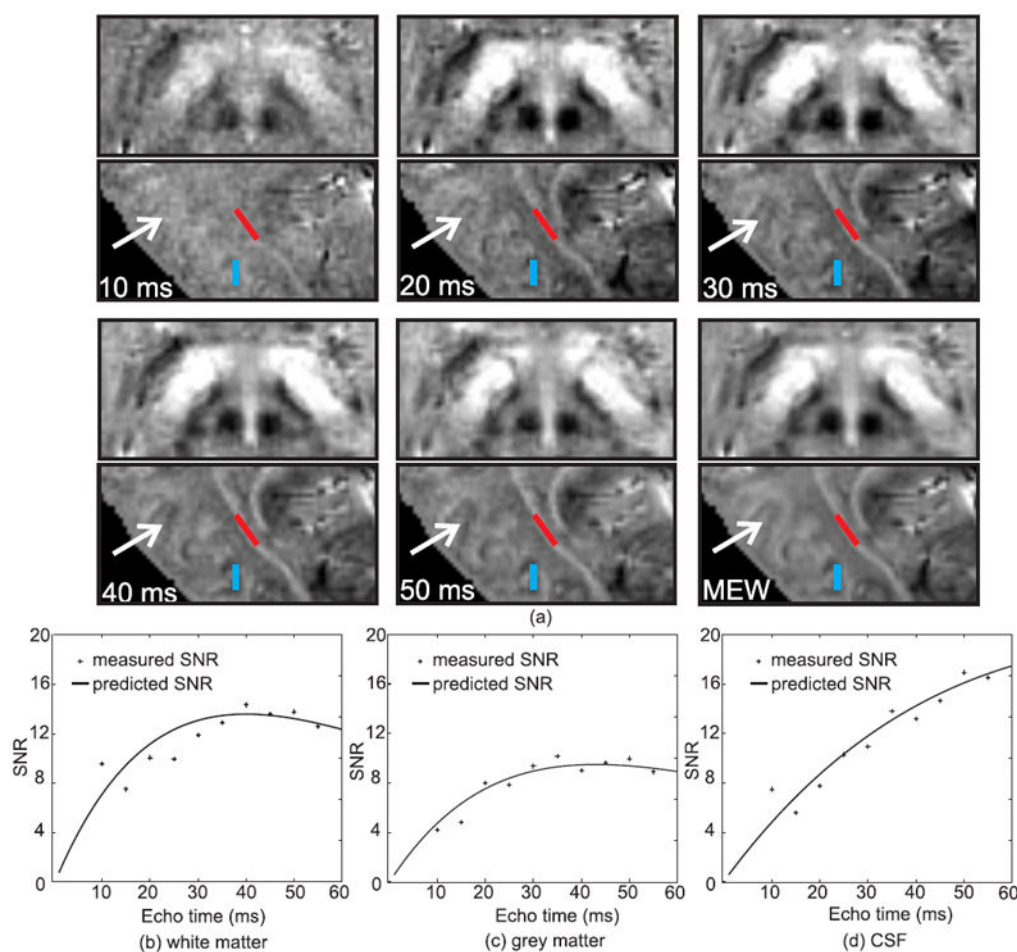
Figure 3.
In vivo demonstration of the behavior of phase SNR. (a) A representative set of frequency maps at echo times of 10, 20, 30, 40 and 50 ms. The SNR gain is clearly visible in the MEW images (arrows). It is also seen that different tissues reaches its maximal SNR at different echo times. (b) SNR of the frequency offsets reaches the optimum at around 40 ms for white matter, (c) around 45 ms for grey matter and (d) longer than 60 ms for CSF. In all three cases (b-d), the experimental measurements agree with theoretical prediction. The selected ROIs in white and grey matters are marked using red and blue colors respectively in (a).
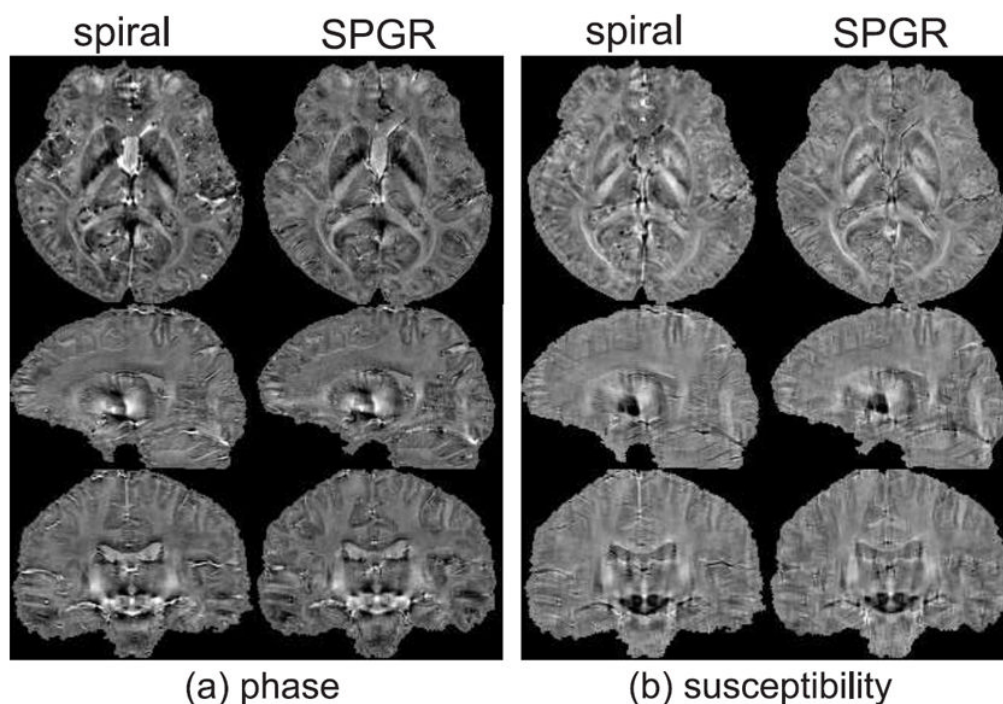
Figure 4.
Comparison of frequency offset and susceptibility maps obtained from multi-echo spiral acquisition and SPGR acquisition: (a) frequency offset map and (b) susceptibility map. phase and susceptibility maps obtained from the two acquisitions have similar levels of SNR and contrast, however spiral acquisition shows a subtle smoothing appearance.
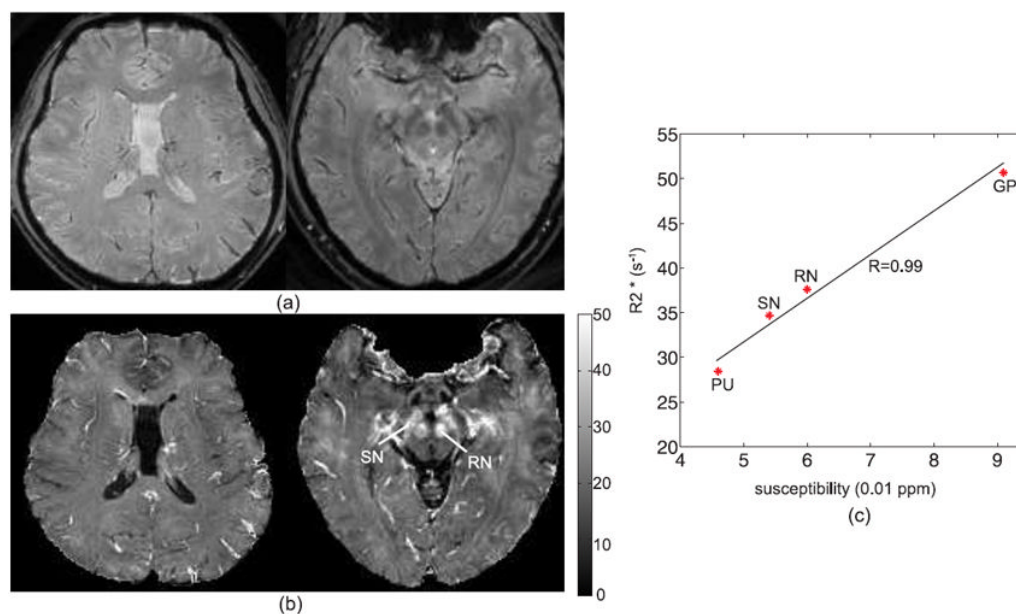
Figure 5.
Examples of simultaneous R2* mapping. (a) Two axial slices of multi-echo magnitude images obtained by combining the magnitude images at different echo times. (b) The corresponding R2* maps. (c) R2* shows a strong correlation with susceptibility in the deep nuclei, as illustrated by the line of best fit as shown.
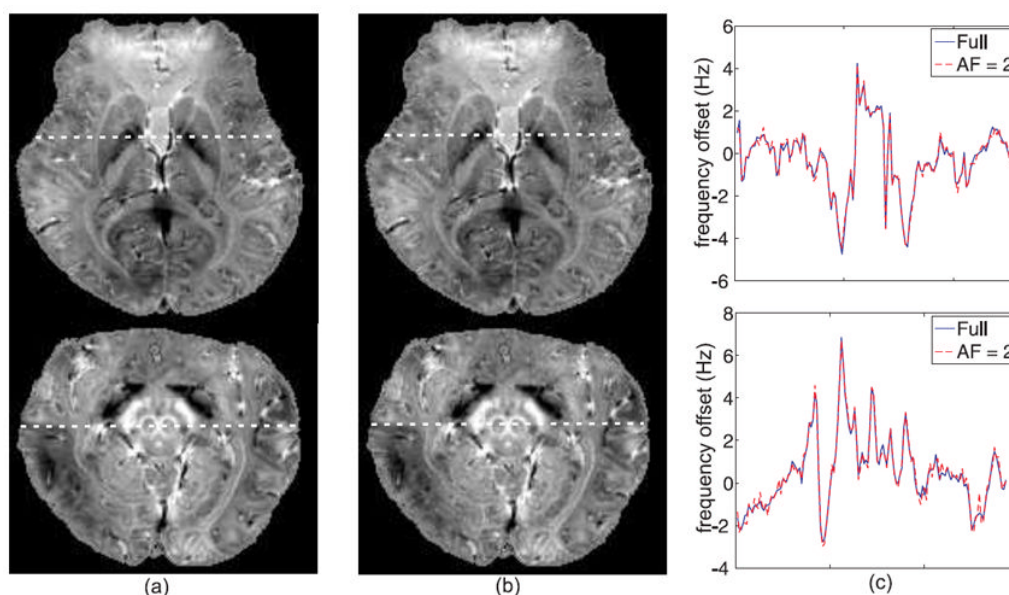
Figure 6.
Comparison of fully sampled and parallel imaging accelerated frequency maps. (a) Multi-echo frequency maps from fully sampled data set. (b) Parallel imaging reconstructed frequency maps with an acceleration factor of 2. (c) Line profiles of the frequency maps show excellent agreement.
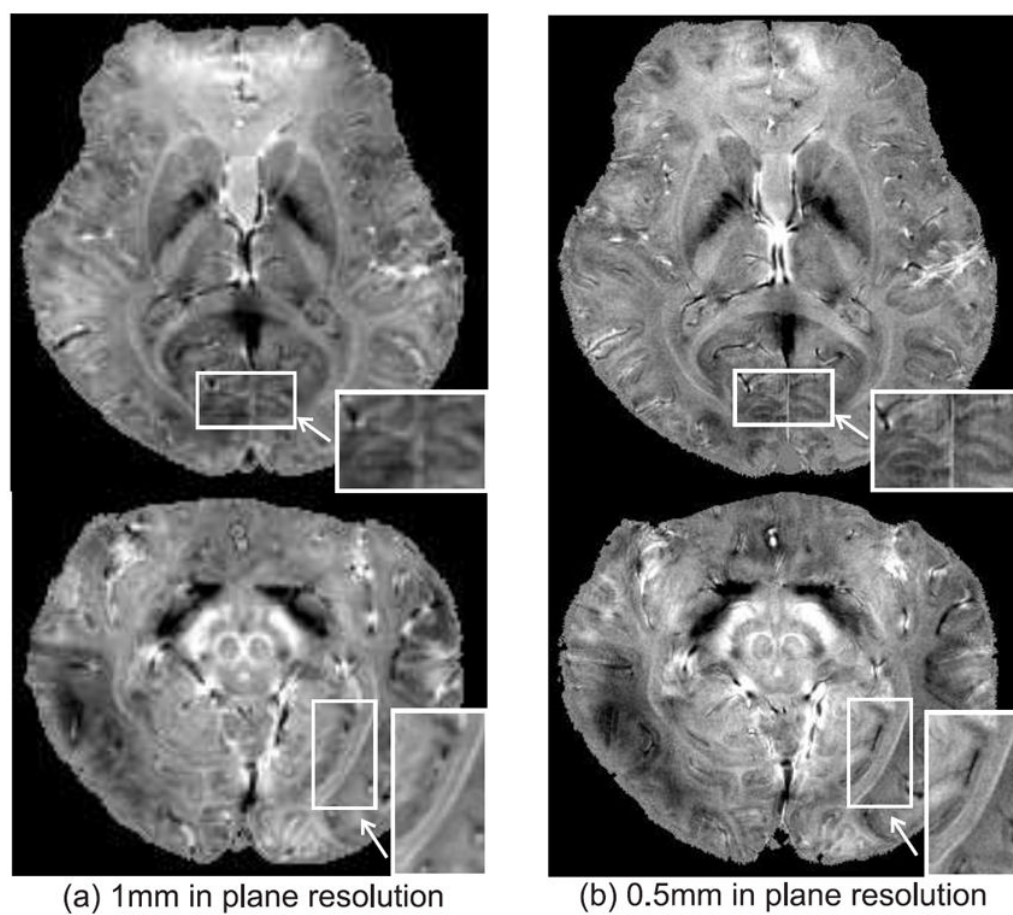
(a) 1mm in plane resolution   (b) 0.5mm in plane resolution

Figure 7.
Comparison of frequency shift maps at (a) 1-mm and (b) 0.5-mm resolution. The enhanced structural details at the 0.5-mm spatial resolution are clearly seen in the zoomed-in regions (insets in the lower corners).

Table 1

Comparison of predicted and measured SNR gain in the frequency map with multi-echo weighted averaging in the ROIs of different brain tissues. [A28]

$\dfrac{SNR_{MEW}}{SNR_{SE}}$	Predicted	Measured
White matter	2.78	2.21
Grey mater	2.72	2.25
CSF	2.39	1.91

Table 2

Comparison of magnetic susceptibility measured with the proposed multi-echo spiral sequence and the standard SPGR sequence.

$x \pm \Delta \times (0.01\ ppm)$	Spiral	SPGR
PU	4.3±0.6	4.7±0.4
SN	5.4±0.6	5.8±0.5
RN	6.1±0.4	6.2±0.5
GP	9.4±1.1	9.0±1.0